GRAVITY WAVES IN MULTILAYER SYSTEMS

Jemma Shipton

supervised by Dr Maarten Ambaum and funded by NERC

Submitted to the Department of Mathematics, University of Reading, in partial fulfilment of the requirements for the Degree of Master of Science.

I confirm that this is my own work and the use of all material from other sources has been properly and fully acknowledged.

Acknowledgements

I would like to thank my supervisor, Maarten Ambaum, for his help and encouragement throughout this project. I am extremely grateful for his guidance and useful suggestions.

Thanks also to my family for their support, and to all the other M.Sc. students for making this year so enjoyable. Special thanks to Dan for cooking me numerous dinners and picking me up from the department whenever I've worked here after dark.

This dissertation and my year of study at Reading University has been financed by the National Environmental Research Council.

Abstract

The generation of gravity waves by topography is examined in this study. These waves are important in the atmosphere on all scales. Their interaction with the mean flow has implications for global atmospheric circulation. They also feature

Contents

List of Figures

Chapter 1

Introduction

1.1 Gravity wave formation

Atmospheric gravity waves are produced when a disturbance causes the air to be displaced from its equilibrium position. Consider an incompressible atmosphere in equilibrium and a fluid parcel of density $\rho(z_0)$ at height z_0. If the parcel is displaced a small distance δz then, assuming it remains intact and does not mix with its surroundings, the parcel will experience a buoyancy force F_b which is given by Archimedes' Law:

$$\mathsf{F}_b = -gv(\rho(z_0) - \rho(z_0 + \delta z))\hat{z}\,, \tag{1.1}$$

where g is the acceleration due to gravity, v is the volume of displaced air which is equal to the volume of the parcel, and $\rho(z_0 + \delta z)$ is the density of the air displaced by the parcel. By Newton's second law of motion

$$\frac{d^2(\delta z)}{dt^2} = -g\frac{\rho(z_0) - \rho(z_0 + \delta z)}{\rho(z_0)}\,. \tag{1.2}$$

Expanding $\rho(z_0 + \delta z)$ as a Taylor series gives

$$\rho(z_0 + \delta z) = \rho(z_0) + \frac{\partial \rho}{\partial z}\Big|_{z=z_0}\delta z + \ldots\,. \tag{1.3}$$

Using this, equation (4.3.2) becomes

$$\frac{d^2\delta z}{dt^2} = \frac{g}{\rho}\frac{\partial \rho}{\partial z}\delta z\,. \tag{1.4}$$

This is the equation for simple harmonic motion. It has the solution

$$\delta z(t) = Ae^{iNt} + Be^{-iNt}, \tag{1.5}$$

where

$$N^2 = -\frac{g}{\rho}\frac{\partial \rho}{\partial z}. \tag{1.6}$$

N is therefore a measure of the stratification of the fluid. For $\partial\rho/\partial z > 0$, the perturbation grows unboundedly and the solution is unstable. If $\partial\rho/\partial z < 0$, N is real and the air parcel oscillates with frequency N. Under these conditions the atmosphere is said to be stably stratified. Gravity waves can have any frequency between 0 and N since the displacements of air parcels within the wave can be at an angle α to the horizontal. In this case the distance δz in (1.4) is replaced by $\sin^2\alpha\delta s$ and N becomes $N = N\sin\alpha$. Typical values of N are $0.01s^{-1}$ in the troposphere and $0.017s^{-1}$ in the stratosphere (Gill, 1982).

So far we have assumed the atmosphere to be incompressible so that density is conserved. A more accurate assumption would be that the atmosphere is adiabatic. In this case it is the potential temperature, $\theta = T\left(p_0/p\right)^{\kappa}$, where p_0 is the surface pressure, that is conserved. However, to a good approximation, the above analysis still holds.

We have seen that disturbances in a fluid can lead to the formation of gravity waves. In the atmosphere these disturbances can be caused by the effects of orography and also by convection and the resulting release of latent heat (Nappo, 2002). In this study the source of the disturbance will be a one dimensional, symmetric, isolated mountain.

1.2 Meteorological applications

Operational forecast models solve an approximation to the full governing equations that filters out gravity waves. This is necessary because the resolution required to explicitly include them would result in an unreasonable execution time. However, the effects of these waves are far from negligible. Gravity waves are important on all scales in the atmosphere. On the large scale gravity wave drag can

slow the mean flow. On a localised scale, gravity waves are associated with lenticular cloud formations and downslope winds such as the Fohn in the Alps and the Chinook in the Rocky mountains. A particularly severe windstorm that has been extensively studied is that which occurred in Boulder, Colorado in January 1969 where wind gusts measured up to 130mph. The strong wind speeds have been attributed to partial reflection of gravity waves from a critical layer aloft. Such layers will be studied in section 4.3.2. A better understanding of the formation and propagation of these waves will lead to better paramaterisation of their effects in global circulation models.

In the next two sections we briefly summarise the local and global effects of gravity waves.

1.2.1 Lee waves

Gravity waves are also the source of some spectacular cloud formations such as those shown in figure 1.1. These lenticular clouds are formed in the lee of mountains. As the air is forced up over the mountain it cools and may reach the dew point temperature in which case the water vapour it contains will start to condense and form droplets. As the air descends again on the other side of the mountain it warms and the water droplets vaporise. However, the continual motion of the airstream means that the water droplets are constantly being replaced so an observer will see a stationary cloud attached to the mountain - only a pilot will experience the dangerous winds within it. If the conditions are such that a standing pattern of lee waves is created, a series of lenticular clouds can form downstream (see figure 1.2).

Due to the stationary appearance of the cloud formations associated with Lee waves, their importance in the atmosphere was not realised until the experiences of gliders and pilots began to reveal the existence of unexplained localised currents near topography. Queney (1948) details the observations that needed explaining:

- strong ascending currents, often to a great height, especially on the upwind side of mountain ranges,

Figure 1.1: A lenticular cloud, courtesy of Jay Shafer, http://vortex.plymouth.edu/lenticular3.html.

- stationary lenticular clouds and cloudless areas in stratocumulous sheets,
- periodical nature of current above large mountain ranges,
- stationary pressure ridges (on crest) and troughs (on lee side),
- formation of intense narrow winds.

The effects can, to a great extent, be explained by the linear theory of internal gravity waves in a stratified fluid. There are two factors that control the development of lee waves: the dimensions of the topography and the characteristics of the airstream. Both must satisfy certain conditions for lee waves to exist and it has been shown (Corby and Wallington, 1956) that the largest amplitude waves occur when the optimum conditions are satisfied by only a small margin.

Scorer (1949) shows that if the airstream satisfies the condition that

$$L^2 = \frac{N^2}{U^2} - \frac{1}{U}\frac{d^2U}{dz^2} \tag{1.7}$$

decreases upwards at a sufficient rate, lee waves will form. For a system consisting

Figure 1.2: A series of lenticular clouds, courtesy of Gary Schultz, http://www.williwaw.com/2001-SEP.html.

of two layers of constant L^2, the condition

$$L_1^2 - L_2^2 > \frac{\pi}{4h^2}, \tag{1.8}$$

where h is the depth of the lower layer, must be satisfied for lee waves to form. Sawyer (1960) shows that, although Scorer's condition is sufficient, it is not necessary and there are other airstream properties that can give rise to lee waves. He demonstrates this by considering the case of a two layer atmosphere in which the top layer is significantly more stable than the lower layer and his numerical results are shown in figure 1.3.

Queney (1948) investigates the conditions of the dimensions of the topography. He shows that, for an airstream with uniform stratification and windspeed, the atmospheric response to a mountain range depends on the half-width a of the range. The main situation of interest to us is that where $a \sim= U/N$, where U and N =g(and)]TJ/F34 2.88 -18.s. 2n(U)]T:7indspee-34b.

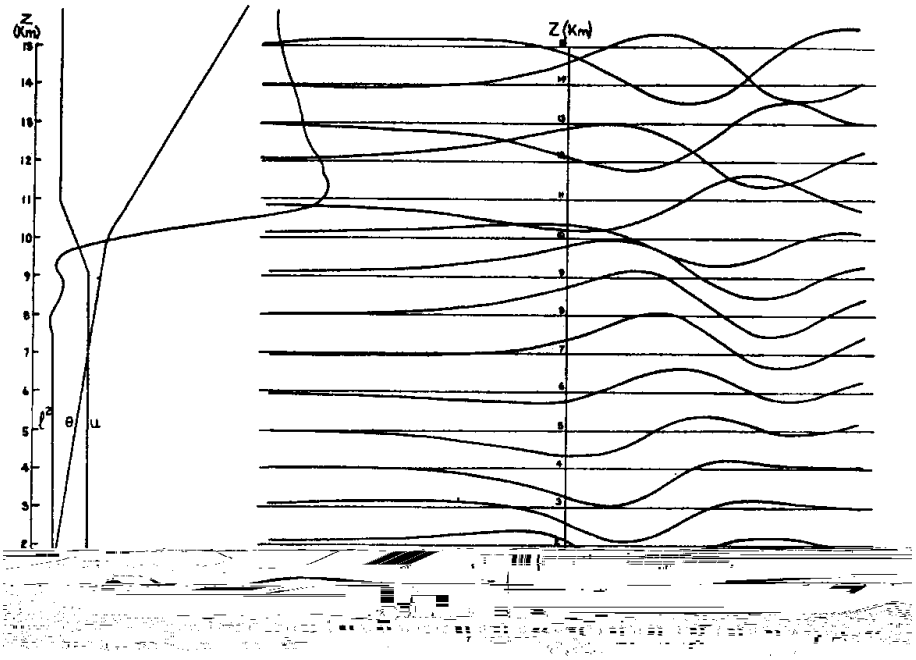

Figure 1.3: Displacement of streamlines computed for an airstream with the vertical profiles of L^2, U and N plotted on the left. A train of rapidly decaying lee waves develops despite the fact that the L^2

In chapter 2 we will examine the flow of a single, homogeneous layer over an obstacle. We will discuss the theory of such a flow and present some results from the one layer model.

Chapter 3 develops the theory of continuously stratified flow. We briefly discuss the energy, momentum and wind stress associated with gravity waves. Wave reflection and trapping will also be investigated.

In chapter 4 we analyse the flow of a multilayer fluid. The governing equations are derived and solved numerically. The multilayer program is tested and the results discussed.

Chapter 5 presents the conclusions and outlines the possibilities for further work.

Chapter 2

The flow of a single homogeneous layer

2.1 The basic equations

Consider a layer of 2-dimensional, incompressible, homogeneous fluid with a free surface flowing over an isolated mountain. The equations of motion for such a fluid with density ρ and pressure p are

$$\frac{D\mathbf{u}}{Dt} = -\frac{1}{\rho}\nabla p - g\hat{\mathbf{z}}, \tag{2.1}$$

$$\nabla.\mathbf{u} = 0, \tag{2.2}$$

where $\mathbf{u} = (u, w)$ is the fluid velocity with components in the Cartesian (x, z) directions and $\hat{\mathbf{z}}$ is the vertical unit vector. At its lower boundary the fluid encounters topography $z = h(x)$ and the condition that there can be no flow though this surface gives

$$w = \mathbf{u}.\nabla h \text{ on } z = h(x). \tag{2.3}$$

The fluid has an upper free surface with mean level $z = \bar{d}$ and displacement $\eta(x)$ as shown in figure 2.1. Assuming the density of any fluid above this surface to be negligible and taking the pressure there to be zero we have

$$w = \frac{D\eta}{Dt} \text{ on } z = \bar{d} + \eta. \tag{2.4}$$

Assuming the vertical accelerations to be small compared to gravity, we can apply the hydrostatic approximation

$$-\frac{1}{\rho}p_z - g = 0. \tag{2.5}$$

Integrating this gives an expression for the pressure

$$p = p_s + \rho g(\bar{d} + \eta - z), \tag{2.6}$$

where p_s is the pressure at the surface. From this equation we can see that p_x is independent of z so if u is initially independent of z it will remain so. Substituting (2.6) into (2.1) gives

$$u_t + uu_x = -g\eta_x. \tag{2.7}$$

This gives us the prognostic equation for the velocity u within the layer. To obtain the prognostic equation for the surface displacement η we need to integrate (2.2) between $z = h$ and $z = \bar{d} + \eta$:

$$0 = \int_{\bar{d}+\eta}^{} \quad \text{and}$$

t5481.7201ny

t5481.725Et801ny

2.2 Linear hydrostatic flow

Consider a steady one dimensional flow with speed U approaching an obstacle of small height as shown in figure 2.1.

Figure 2.1: Definition diagram for the notation in the single layer case. U and $\bar{d}$ are respectively the upstream constant speed and depth, $\eta(x)$ is the displacement of the free surface and $h(x)$ is the topography. $d(x) = \bar{d} + \eta(x) - h(x)$ is the total depth of the fluid layer.

Under these conditions we can set $u(x) = U + u'(x)$ and assume $u'(x), \eta(x)$ and $h(x)$ to be small perturbations. Substituting into (2.7) and (2.11) and linearising gives

$$u'_t + Uu'_x = -g\eta_x, \tag{2.12}$$

$$\eta_t + U\eta_x + \bar{d}u'_x = Uh_x. \tag{2.13}$$

Eliminating u' leaves

$$\left(\frac{\partial}{\partial t} + U\frac{\partial}{\partial x}\right)^2 \eta - c^2\frac{\partial^2\eta}{\partial x^2} = U^2\frac{\partial^2 h}{\partial x^2}, \tag{2.14}$$

where $c = \sqrt{g\bar{d}}$ is the wave speed. With initial conditions $\eta = 0$ and $\eta_t = 0$, 2.14 has solution

$$\eta = \frac{F_0^2}{F_0^2 - 1}h(x) - \frac{F_0}{2}\left[\frac{1}{F_0 + 1}h\left(x - (U + c)t\right) + \frac{1}{F_0 - 1}h\left(x - (U - c)t\right)\right] \tag{2.15}$$

when the initial Froude number $F_0 = U/c \neq 1$. This solution, for $F_0 < 1$ is shown in figure 2.2. It is made up of a steady component over the obstacle and two propagating waves which are functions of the characteristic variables. All three terms have the same form as the obstacle but with different amplitudes which depend solely on the initial conditions.

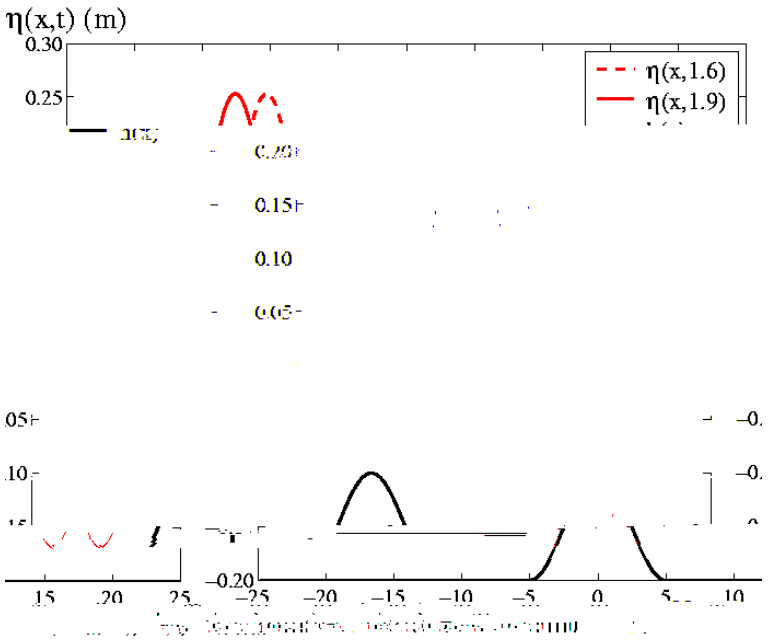

Figure 2.2: Example of the linear solution for flow over an obstacle.

For $F_0 < 1$ the upstream propagating wave has larger amplitude. The two types of flow are shown in figures 2.3 and 2.4.

2.3 Nonlinear hydrostatic flow

The linear equations are only valid for sufficiently small h_{max}. When h_{max} does not satisfy this constraint, nonlinear effects become apparent and can even dominate the system. One important nonlinear phenomenon is the hydraulic jump or shock. Although this study will be restricted to cases where there are no shocks, it is important to know the circumstances under which they form so that they can

be avoided. Consider the case shown in figure 2.5 where the wave initially has a small amplitude but, as the deeper fluid moves faster, the interface steepens and may become vertical. This is the shock which, if required, can be modelled as a discontinuity. At a shock, the flow changes from supercritical to subcritical or vice-versa and this suggests that the local Froude number at this point must be unity. This is shown to be true later on in this section.

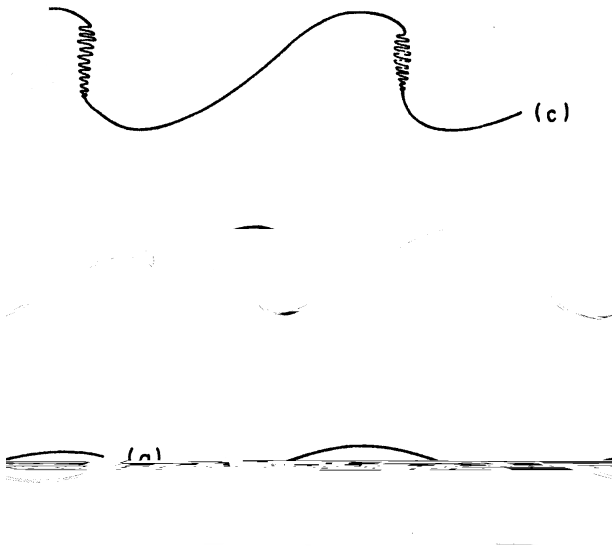

Figure 2.5: This diagram illustrates the formation of a shock wave. The initial wave is that labelled (a). As its amplitude increases the profile steepens until, as in case (c), the wave breaks. Adapted from Andrews and Leovy. (1987).

Following Houghton and Kasahara (1968) we examine the steady state equa-

which, when integrated, give

$$\frac{1}{2}u^2 + g(d+h) = \frac{1}{2}U^2 + g\bar{d}, \tag{2.18}$$

$$ud = U\bar{d}. \tag{2.19}$$

Using (2.19) to eliminate u from (2.18) gives

$$\frac{1}{2}U^2\frac{\bar{d}^2}{d^2} + g(d+h) = \frac{1}{2}U^2 + g\bar{d}, \tag{2.20}$$

which can be rewritten in terms of the dimensionless variables $F_0 = U/c$, $D = d/\bar{d}$ and $H = h/\bar{d}$ as

$$D^3 + \left(H - \frac{1}{2}F_0^2 - 1\right)D^2 + \frac{1}{2}F_0^2 = 0. \tag{2.21}$$

Figure 2.6 shows this polynomial, plotted as a function of D, for $F_0 = 0.5$ and three different values of H. Since $F_0 < 1$ the fluid will dip over the obstacle so $d < \bar{d}$ and $D < 1$ and the root of the polynomial corresponding to the physical solution is that between 0 and 1. Figure 2.7 shows the same polynomial for $F_0 = 1.5$. In this case the fluid rises over the obstacle and the root we are interested in is the first which is greater than 1. In both cases, it can be seen that for H greater than some critical value H_{crit}, there is no physically meaningful solution. Having demonstrated this graphically we now give a mathematical argument. Defining the function

$$g(D, F_0, H) = D^3 + \left(H - \frac{1}{2}F_0^2 - 1\right)D^2 + \frac{1}{2}F_0^2, \tag{2.22}$$

we see that for there to be a solution to $g = 0$ for a given height H, we must have

$$\delta g = \frac{\partial g}{\partial F_0}\delta F_0 + \frac{\partial g}{\partial D}\delta D = 0. \tag{2.23}$$

Except in the trivial case $D = 1$ which corresponds to the solution for flow over a flat horizontal boundary, $\partial g/\partial F_0 = F_0(1 - D^2)$ is non-zero. Thus any small change in F_0 must be balanced by a small change in D. This can only occur if $\partial g/\partial D \neq 0$. This condition gives us an equation for the critical depth D_{crit}. Calculating the partial derivative of g with respect to D gives

$$\frac{\partial g}{\partial D} = 3D^2 + 2D\left(H - \frac{1}{2}F_0^2 - 1\right). \tag{2.24}$$

This is zero when

$$D = D_{crit} = -\frac{2}{3}(H - \frac{1}{2}F_0^2 - 1)\,. \tag{2.25}$$

Imposing the condition $g(D_{crit}, F_0, H) = 0$ gives

$$D_{crit}^3 = F_0^2\,. \tag{2.26}$$

So we have found an expression for the critical depth at which $g = 0$ has no solutions. We now use this to find an equation for the critical mountain height. Rearranging (2.18) gives

$$D^3 = \frac{F_0^2}{F^2}\,, \tag{2.27}$$

where $F = u/\sqrt{gd}$. Comparing this with (2.26), shows that the local Froude number F^2 must be unity at the critical point. Setting $F^2 = 1$ in (2.26) and substituting this into (2.21) gives, after some rearrangement,

$$H_{crit} = 1 + \frac{1}{2}F_0^2 - \frac{3}{2}F_0^{2/3}\,. \tag{2.28}$$

This function is plotted in figure 2.8. Long has shown (Long, 1954) that any H greater than H_{crit} will cause the solution to become discontinuous, so $h_{crit} = H_{crit}\bar{d}$ is the maximum height of the mountain for which the flow does not contain shocks. In this study we will restrict our attention to mountains with $h_{max} < h_{crit}$, the shaded area in figure 2.8.

The introduction of shocks is not the only effect of using the full nonlinear equations. Some steepening of the waves is still likely even if a shock is not finally formed.

2.3.1 The program

The program single_layer_program.f90 solves equations (2.7) and (2.11) for U, $\bar{d}$ and h_{max} as input by the user. Since we do not wish to analyse shocks it is not necessary to use a shock fitting or shock capturing method. Instead the program uses a simple leapfrog method which solves

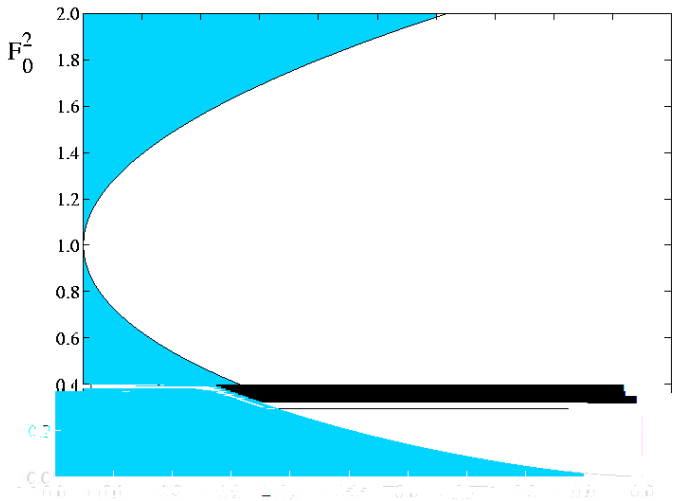

Figure 2.8: The non-dimensional maximum height of the mountain, H_{max}, as a function of the initial Froude number, F_0^2

$$u_j^{n+1} = u_j^{n-1} - \frac{dt}{dx}\left(F_{j+1}^n - F_{j-1}^n\right), \tag{2.29}$$

$$\eta_j^{n+1} = \eta_j^{n-1} - \frac{dt}{dx}\left(K_{j+1}^n - K_{j-1}^n\right), \tag{2.30}$$

where

$$F_j^n = \frac{1}{2}(u_j^n)^2 + g\eta_j^n, \tag{2.31}$$

$$K_j^n = u_j^n(\bar{d} + \eta_j^n - h_j), \tag{2.32}$$

and q_j^n denotes the value of variable q at (x_j, t^n). In order to study the steady state solution we require the transient waves to leave the domain. This is easily accomplished by including a wave absorbing, or sponge, layer at the lateral boundary. We define the Rayleigh damping function $\lambda(x)$ to be zero everywhere except in a narrow region near the boundary. Including this damping function alters the governing equations (2.7) and (2.11) to

$$u_t + F_x = -\lambda(x)(u - U), \tag{2.33}$$

$$\eta_t + K_x = -\lambda(x)\eta\,, \tag{2.34}$$

where F_x and K_x are the continuous fluxes corresponding to F_j^n and K_j^n above. Discretising these equations gives

$$u_j^{n+1} = u_j^{n-1} - \frac{dt}{dx}\left(F_{j+1}^n - F_{j-1}^n\right) - 2dt\lambda_j(u_j^{n+1} - U)\,, \tag{2.35}$$

$$\eta_j^{n+1} = \eta_j^{n-1} - \frac{dt}{dx}\left(K_{j+1}^n - K_{j-1}^n\right) - 2dt\lambda_j\eta_j^{n+1}\,. \tag{2.36}$$

These are implicit equations which are usually solved using matrix inversion techniques. However, such complications do not arise here as (2.35) and (2.36) can easily be rearranged to give

$$u_j^{n+1} = \frac{1}{1 + 2dt\lambda_j}\left(u_j^{n-1} - \frac{dt}{dx}\left(F_{j+1}^n - F_{j-1}^n\right) + 2dtU\lambda_j\right)\,, \tag{2.37}$$

$$\eta_j^{n+1} = \frac{1}{1 + 2dt\lambda_j}\left(\eta_j^{n-1} - \frac{dt}{dx}\left(K_{j+1}^n - K_{j-1}^n\right)\right)\,. \tag{2.38}$$

Since we will be dealing with large amplitude waves it is likely that we will encounter problems due to nonlinear instability. This can be kept under control by including some form of artificial diffusion. In this program the diffusion process will be performed at the end of each timestep by simply averaging u^n and η^n according to the formula

$$q_j^n = \left(1 - \frac{av}{2}\right)q_j^n + \frac{av}{4}\left(q_{j+1}^n + q_{j-1}^n\right)\,. \tag{2.39}$$

2.3.2 Sensitivity to parameters

The Courant-Friedrichs-Levy condition states that we must have

$$dt < \frac{dx}{c}\,. \tag{2.40}$$

However, this condition only ensures stability for linear equations. Since we are solving nonlinear equations the condition on dt is more restrictive and it has been found, for the programs used in this study, that

$$dt < \frac{dx}{4c}\,. \tag{2.41}$$

Despite keeping dt small enough to ensure that the scheme remains stable, nonlinear instabilities still cause spurious oscillations in the solution. Instead of reducing dt further, which would result in longer run times, we introduce the av parameter described above. This smooths the solution and prevents the errors from building up. However, it can also reduce the maximum amplitudes of the waves. The optimum value of av is different in each situation depending on how close the mountain is to critical height. If h_{max} is sufficiently small for the linear approximation to be applicable, av can be set to zero, even though we are solving the nonlinear equations. However, as h_{max} is increased, av is progressively more important. We have considered each situation individually in this study and the results presented are those for which av is set to the minimum value for stability.

2.3.3 Results

To begin with we test the program against some results from Houghton and Kasahara (1968) who in turn have compared their results to the experiments of Long (1954). The obstacle shape is given by

$$h(x) = h_{max} \quad 1$$

Houghton and Kasahara (1968). Houghton and Kasahara (1968) used a scheme developed by Lax and Wendroff which, unlike the Leapfrog scheme used here, is capable of handling shocks. Although we will not study flows containing shocks, it is interesting to see how the program copes with these situations. In fact, as shown in figures 2.11 and 2.12, it does surprisingly well. The general shape of the solution is as given in figures 14b and 14c of Houghton and Kasahara (1968) and the discontinuities are captured well with the exception of the upstream travelling jump in figure 2.11. Some oscillations are evident in the region of the discontinuities but this is to be expected - even the Lax-Wendroff code used in Houghton and Kasahara (1968) does this. The Leapfrog scheme remains stable by virtue of the averaging process explained in the previous section. With this switched off the program is unable to cope with the discontinuities and is soon outputting infinite values. The results in these four figures were produced with av set to 0.01. For values higher than this the solutions were considerably smoother with some discontinuities hardly apparent. For values lower than 0.01 the oscillations at the discontinuities were worse.

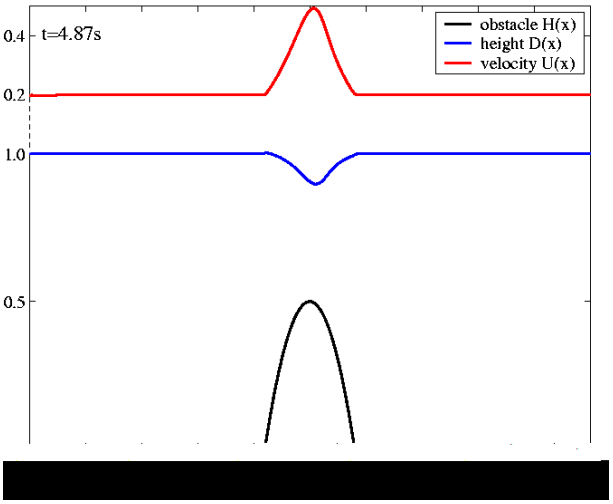

Figure 2.9: $F_0 = 0.2$. This figure corresponds to figure 14a in Houghton and Kasahara (1968).

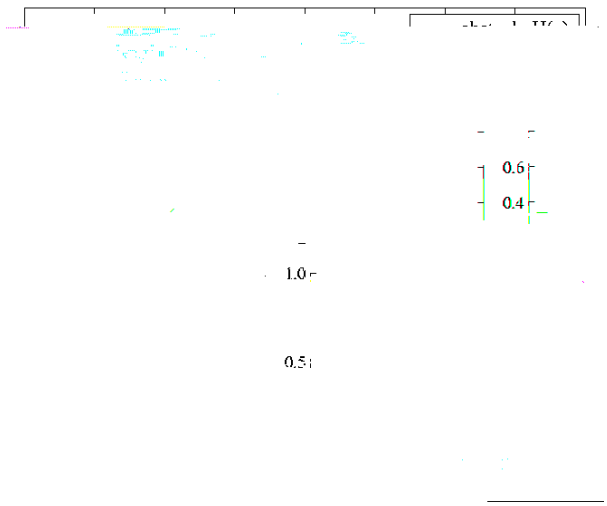

Figure 2.11: $F_0 = 0.3$. This figure corresponds to figure 14b in Houghton and Kasahara (1968). The height of the free surface (blue) and the velocity (red) are shown in the dimensionless units $D = d/\bar{d}$ and U

Having looked at the case where nonlinear effects are most important, we now turn our attention to the other extreme: the linear case. The following results are computed for length scales appropriate for the atmosphere rather than, as previously, for comparison with experiment. A scaled down version of the mountain has been included in each plot. The mountain scaling is the same in all three figures but the waves in figure 2.13 have been scaled up for clarity.

We can see from figure 2.13 that for a mountain of height $h_{max} = 100m = 0.1\bar{d}$ the linear and nonlinear solutions are almost indistinguishable with particu-

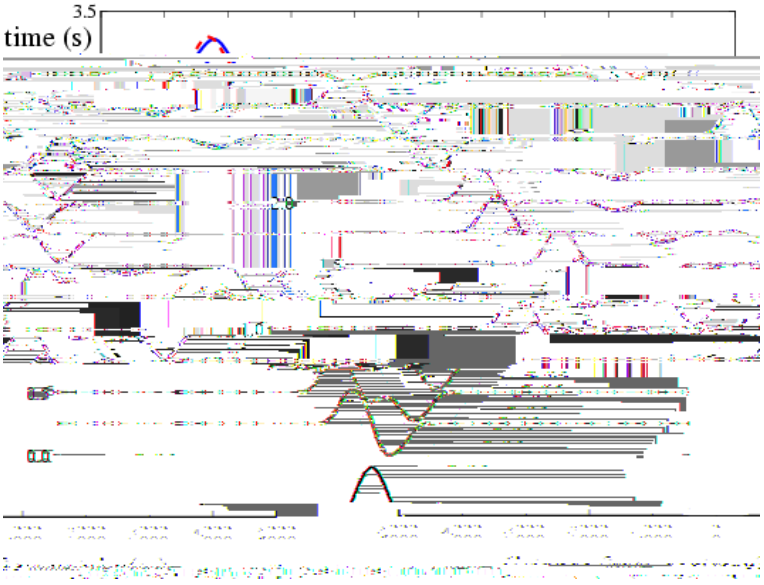

Figure 2.13: x-t diagram of the numerical solution (blue) compared to the exact linear solution (red) for the case were $h_{max} \ll h_{crit}$

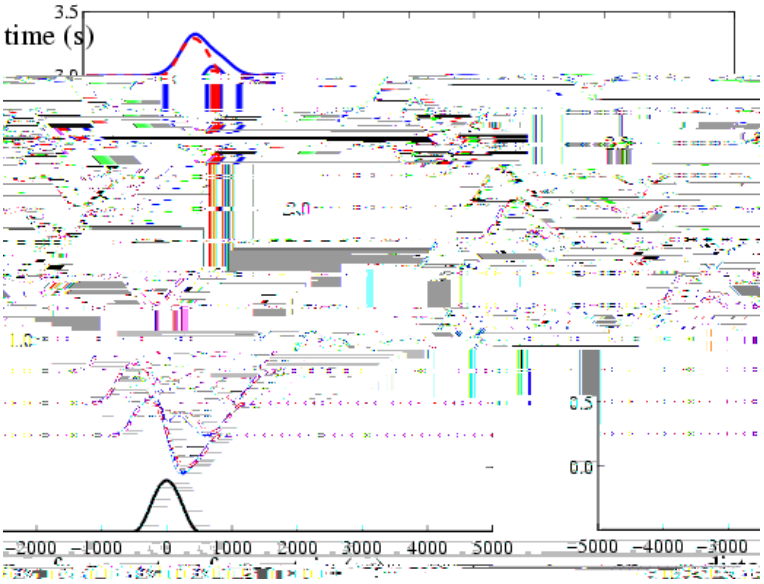

Figure 2.14: x-t diagram of the numerical solution (blue) compared to the exact linear solution (red) for the case where $h_{max} < h_{crit}$

Chapter 3

Stratified flow

these equations to give:

$$\left(\frac{\partial}{\partial t} + U\frac{\partial}{\partial x}\right)u + w\frac{dU}{dz} = -\frac{1}{\rho_0}\frac{\partial p}{\partial x}, \tag{3.2}$$

$$\left(\frac{\partial}{\partial t} + U\frac{\partial}{\partial x}\right)w = -\frac{1}{\rho_0}\frac{\partial p}{\partial z} - \frac{\rho}{\rho_0}g, \tag{3.3}$$

$$\frac{\partial u}{\partial x} + \frac{\partial w}{\partial z} = 0, \tag{3.4}$$

$$\left(\frac{\partial}{\partial t} + U\frac{\partial}{\partial x}\right)\rho + w\frac{d\rho_0}{dz} = 0. \tag{3.5}$$

Taking the x derivative of (3.2) and substituting for $\partial u/\partial x$ from (3.4) gives

$$\left(\frac{\partial}{\partial t} + U\frac{\partial}{\partial x}\right)\frac{\partial w}{\partial z} - \frac{dU}{dz}\frac{\partial w}{\partial x} = \frac{1}{\rho_0}\frac{\partial^2 p}{\partial x^2}. \tag{3.6}$$

Eliminating ρ from (3.3) using (3.5) leaves

$$\left(\frac{\partial}{\partial t} + U\frac{\partial}{\partial x}\right)^2 w + N^2 w = -\frac{1}{\rho_0}\left(\frac{\partial}{\partial t} + U\frac{\partial}{\partial x}\right)\frac{\partial p}{\partial z}. \tag{3.7}$$

Adding $\left(\frac{\partial}{\partial t} + U\frac{\partial}{\partial x}\right)\frac{\partial}{\partial z}$(3.6) to $\frac{\partial^2}{\partial x^2}$(3.7), treating ρ_0 as constant in (3.6), removes p, leaving an equation for w:

$$\left(\frac{\partial}{\partial t} + U\frac{\partial}{\partial x}\right)^2\left(\frac{\partial^2}{\partial x^2} + \frac{\partial^2}{\partial z^2}\right)w + N^2\frac{\partial^2 w}{\partial x^2} - \frac{d^2U}{dz^2}\left(\frac{\partial}{\partial t} + U\frac{\partial}{\partial x}\right)\frac{\partial w}{\partial x} = 0. \tag{3.8}$$

By treating ρ_0 as constant in (3.6) we have assumed that density variations are negligible compared to the other terms in the momentum equations but we have retained the density variation when it gives rise to a buoyancy force. This approximation is known as the Boussinesq approximation and it is applicable when the vertical scale of the motion is much less than the density scale height of the atmosphere (Nappo, 2002). If we assume that the motion is steady then this equation can be integrated twice with respect to x:

$$\frac{\partial^2 w}{\partial x^2} + \frac{\partial^2 w}{\partial z^2} + \left(\frac{N^2}{U^2} - \frac{1}{U}\frac{d^2U}{dz^2}\right)w = 0. \tag{3.9}$$

Assuming a wave like solution of the form

$$w(x,z) = \hat{w}(z)e^{ikx}, \tag{3.10}$$

gives

$$\frac{\partial^2 \hat{w}}{\partial z^2} + \left(\frac{N^2}{U^2} - \frac{1}{U}\frac{d^2 U}{dz^2} - k^2 \right) \hat{w} = 0. \tag{3.11}$$

This has solution, for each k,

$$\hat{w}(k, z) = \hat{w}(k, 0) e^{-imz}, \tag{3.12}$$

where

$$m = \left(\frac{N^2}{U^2} - \frac{1}{U}\frac{d^2 U}{dz^2} - k^2 \right)^{1/2}. \tag{3.13}$$

The sign of m has been chosen so that the energy propagates upward. To ob-

Using (3.4) we can write

$$u\frac{\partial p}{\partial x} + w\frac{\partial p}{\partial z} = \frac{\partial u\,p}{\partial x} + \frac{\partial w\,p}{\partial z}. \tag{3.17}$$

Substituting this into (3.16) gives

$$\frac{D}{Dt}\left[\rho_0(u^2+w^2)\right] + \rho\, w\, g = -\frac{\partial u\,p}{\partial x} - \frac{\partial w\,p}{\partial z} - \rho_0 u\, w\,\frac{dU}{dz}. \tag{3.18}$$

From (3.5) we see that

$$\rho\, w\, g = -\frac{\rho\, g}{\rho_{0z}}\frac{D\rho}{Dt} = \frac{g^2}{2\rho_0 N^2}\frac{D\rho^2}{Dt}. \tag{3.19}$$

(3.19) then becomes

$$\frac{D}{Dt}\left[\rho_0(u^2+w^2) + \frac{g^2}{2\rho_0 N^2}\rho^2\right] = -\frac{\partial u\,p}{\partial x} - \frac{\partial w\,p}{\partial z} - \rho_0 u\, w\,\frac{dU}{dz}. \tag{3.20}$$

It is clear that

$$\frac{D}{Dt}\left[\rho_0(u^2+w^2)\right] \tag{3.21}$$

is the total rate of change of perturbation kinetic energy. It is not so clear that

$$\frac{D}{Dt}\left[\frac{g^2}{2\rho_0 N^2}\rho^2\right] \tag{3.22}$$

is the total rate of change of the perturbation potential energy. To see this we consider the gravitational potential energy PE gained by a fluid parcel when it is vertically displaced from its equilibrium position by a distance h. Denoting the buoyant force per unit volume by F_b we have

$$\begin{aligned} PE &= -\int_0^h F_b\,dz && (3.23)\\ &= -\int_0^h g\frac{d\rho_0}{dz}z\,dz && (3.24)\\ &= -\frac{1}{2}\frac{d\rho_0}{dz}gh^2 && (3.25)\\ &= -\frac{1}{2}\rho_0 N^2 h^2 && (3.26)\\ &= \frac{1}{2}\frac{g^2}{\rho_0}\frac{\rho^2}{N^2}, && (3.27) \end{aligned}$$

where

$$\rho = \rho_0(z) - \rho_0(z + h) \approx -h\frac{d\rho_0}{dz}. \tag{3.28}$$

So we have seen that the left hand side of (3.20) represents the total rate of change of the perturbation energy. Examining the right hand side of this equation shows us what this change is due to. up and wp are the fluxes of wave energy in the horizontal and vertical directions respectively so the first two terms on the right hand side are the divergences of these fluxes. The final term is zero if there is no background wind shear and, if the buoyancy frequency is constant, wave perturbation energy is conserved.

3.4 Wave reflection, trapping and resonance

Atmospheric properties such as wind speed and buoyancy frequency change with height and if the change is sharp enough, such as at an inversion, vertically propagating waves may not be able to penetrate the layer and are instead reflected back down. In some cases the wave is only partially reflected, the rest of the wave being transmitted through the layer. Just as before this wave can be either propagating or evanescent. The lower layer now contains both upwards and downwards propagating waves and, depending on their wavelength and the height of the reflecting layer, they can either destructively or constructively interfere. Constructively interfering waves are trapped below the reflecting layer and are capable of transporting energy a considerable distance downstream. The continual generation of energy by the mountain can lead to resonance and this phenomenon explains the existence of strong downslope winds.

Typical vertical profiles of wind speed and buoyancy frequency in the atmosphere are complicated so for simplicity we consider the case of piecewise continuous Scorer parameter, L^2. This is a generalisation of the theory given in Gill (1982) and Nappo (2002) for piecewise continuous buoyancy frequency.

There are four possible forms of solution since we can have either propagating or evanescent waves in each layer. In the lower layer it is possible to have both upward propagating waves generated by the boundary and downward propagating waves reflected from the discontinuity in L^2. In the upper layer only waves propagating upward are possible. Thus

$$\begin{aligned} w &= A^{refr} e^{im_2(z-H)} e^{-i(kx-\omega t)}, z > H, \\ w &= \left(A^{in} e^{im_1(z-H)} + A^{refl} e^{-im_1(z-H)} \right) e \end{aligned} \tag{3.33}$$

where we have defined the reflection coefficient r as the ratio of the amplitude of upward and downward propagating waves

$$r = \frac{A^{refl}}{A^{in}}. \tag{3.36}$$

We can find r by applying the conditions that the perturbation pressure p and the vertical velocity w are continuous across the interface. However, following Gill (1982) and Nappo (2002) this is simplified if we define the impedance $Z = \frac{p'}{\rho_0 w'}$. Since p and w are continuous across the interface, Z must also be. To calculate Z in each layer we must first calculate the perturbation pressure p. To do this we assume wave like solutions of the form $q(x, z, t) = \tilde{q}(z)e^{i(kx-\omega t)}$ for each of the variables u, ρ, p and w

Applying the condition that Z is continuous across the boundary gives

$$\frac{m_2}{m_1} = \frac{1-r}{1+r}. \tag{3.46}$$

Rearranging this as

$$r = \frac{m_1 - m_2}{m_1 + m_2} \tag{3.47}$$

gives us some information about the properties of the waves in each layer. By definition, if $r = 0$ the wave will be propagating in both layers and $m_1 = m_2$. It is also clear from the definition of r that if $|r| = 1$ there is total reflection and the wave is trapped in the bottom layer. If $r = 1$ then m_2 must be zero and the wave cannot propagate through the upper layer.

3.5 The hydrostatic approximation

In this section we examine the consequences of making the hydrostatic approximation. As we shall see in the next chapter, this approximation is essential for the formulation of the multilayer atmospheric model. Therefore we must understand the implications that the assumption of hydrostatic balance has on the flow.

The hydrostatic approximation imposes restrictions on the scale of flow to which the model can be applied. Following Gill (1982) we substitute (3.2) into the time derivative of (3.4) to obtain

$$\frac{\partial^2 w}{\partial z \partial t} = \frac{1}{\rho_0}\frac{\partial^2 p}{\partial x^2}. \tag{3.48}$$

If we assume plane wave solutions this gives the relation

$$p = -\frac{m}{k^2}\omega\rho_0 w_0 \cos(kx + mz - \omega t), \tag{3.49}$$

and (3.5) gives

$$\rho = -\frac{N^2}{\omega g}\rho_0 w_0 \sin(kx + mz - \omega t). \tag{3.50}$$

Setting $U = 0$ in (3.8) gives the dispersion relation

$$\omega^2 = \frac{N^2 k^2}{k^2 + m^2}, \tag{3.51}$$

Chapter 4

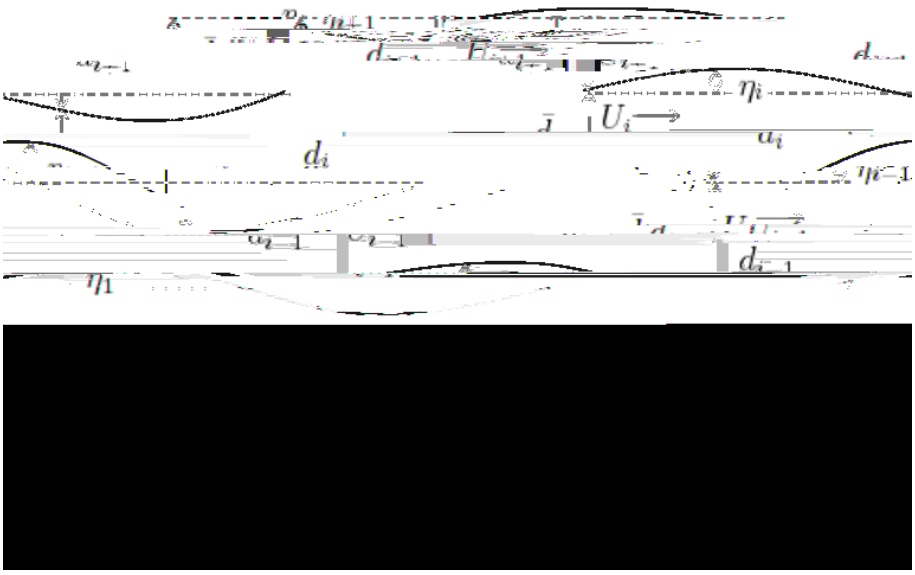

Figure 4.1: Definition diagram for the notation in the multilayer case. U_i and $\bar{d}_i$ are respectively the upstream constant speed and depth in the i^{th} layer, $\eta_i(x)$ is the displacement of the i^{th} interface and $h(x)$ is the topography. $d_i(x) = \bar{d}_i + \eta_i(x) - \eta_{i-1}(x)$ is the total depth of the i^{th} fluid layer.

Integrating this from a point z_i within the i^{th} layer to the top of the layer gives

$$p_i(z_i) =$$

If we impose the condition that the pressure is continuous across each interface so that

$$p_{is} = p_i\left(\sum_{j=1}^{i}\bar{d}_j + \eta_i\right) = p_{i+1}\left(\sum_{j=1}^{i}\bar{d}_j + \eta_i\right), \tag{4.7}$$

we can rewrite (4.6) as

$$p_{l-1}(z_{l-1}) = p_l\left(\sum_{j=1}^{l-1}\bar{d}_j + \eta_{l-1}\right) + g\rho_{l-1}\left(\sum_{j=1}^{l-1}\bar{d}_j + \eta_{l-1} - z_{l-1}\right). \tag{4.8}$$

Using (4.5) we see that

$$p_{l-1}(z_{l-1}) = p_s + g\left[\rho_l(\bar{d}_l + \eta_l - \eta_{l-1}) + \rho_{l-1}\left(\sum_{j=1}^{l-1}\bar{d}_j + \eta_{l-1} - z_{l-1}\right)\right]. \tag{4.9}$$

Continuing this process we see that the general equation for the pressure in the i^{th} layer is

$$p_i(z_i) = p_s + g\left[\sum_{j=i+1}^{l}\rho_j(\bar{d}_j + \eta_j - \eta_{j-1}) + \rho_{l-1}\left(\sum_{j=1}^{i}\bar{d}_j + \eta_i - z_i\right)\right]. \tag{4.10}$$

Substituting this into (4.1) and taking the surface pressure to be zero gives

$$u_{it} + u_i u_{ix} = -g\left[\frac{1}{\rho_i}\sum_{j=i+1}^{l}\rho_j(\eta_{jx} - \eta_{(j-1)x}) + \eta_{ix}\right]. \tag{4.11}$$

a leapfrog scheme with a sponge layer to absorb the waves at the lateral boundary. The same process of numerical diffusion is also included. The only complication encountered in the multilayer case is the presence of an upper boundary. There is no such distinct upper boundary in the atmosphere. Therefore, we require an upper boundary condition that enables the waves to propagate out of the domain. This is accomplished by adding another sponge layer, this time to the top of the domain. The second damping function, $\lambda_2(x)$ is plotted in green in figure 4.2. The discrete equations solved by this program are

$$u_{i,j}^{n+1} = \frac{u_{i,j}{}^{n-1} - \frac{dt}{dx}(F_{i,j+1}^{n} - F_{i,j-1}^{n}) + 2dt(\lambda_{i,j} + \lambda_{2,i,j})U_i}{1 + 2dt(\lambda_{2,i,j} + \lambda_{i,j})}, \quad (4.14)$$

$$\eta_{i,j}^{n+1} = \frac{\eta_{i,j}^{n-1} - \frac{dt}{dx}(K_{i,j+1}^{n} - K_{i,j-1}^{n})}{1 + 2dt(\lambda_{2,i,j} + \lambda_{i,j})}. \quad (4.15)$$

As in the single layer case, we require some numerical diffusion to keep the scheme stable. This is accomplished in the same way as before.

4.2.1 Sensitivity to parameters

The same conditions as outlined in section (2.3.2) apply to *dt* and *av* in this multilayer program. However, since we are now attempting to model a continuously stratified fluid by a set of discrete layers, we need to consider the vertical resolution, that is, the number of layers of constant density used to model a layer of

$$= \quad -g\frac{\rho_2}{\rho_1}\eta_{2x} - g\,\eta_{1x} \tag{4.21}$$

we see that if η_{2x} is relatively small, the motion in the lower layer is similar to that in a single layer with reduced gravity

$$g \;= 1 - \frac{\rho_2}{\rho_1}\,. \tag{4.22}$$

If we make the rigid lid approximation $\eta_{2x} = 0$, the two cases become identical. This can be seen in figure 4.3.

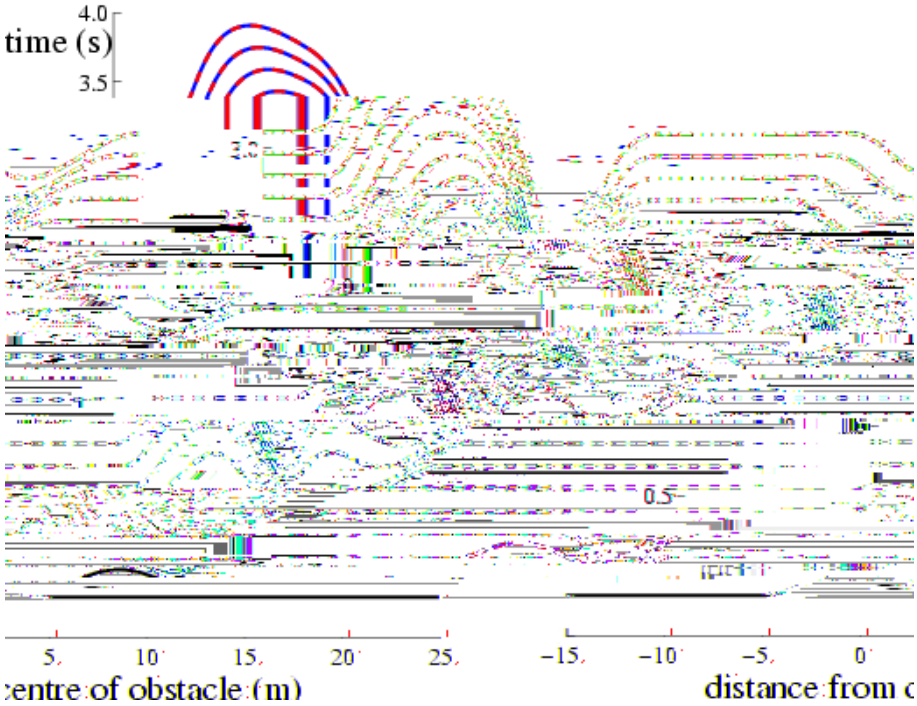

Figure 4.3: Two layer flow showing the solution for the lower layer (blue) compared to the solution for a single layer system with reduced gravity g .

4.3.2 Partial reflection

Klemp and Lilly (1975) study a linear hydrostatic model of the atmosphere comprising three layers of buoyancy frequency. Their aim is to investigate the atmospheric conditions which produce intense surface winds. We aim to reproduce

their result (see figure 4.5) which shows partial reflection of the wave and a significant increase in wave amplitude in the lower layer. The values given in Klemp and Lilly (1975) for their three layers are

$$N_1 = 1.6 \times 10^{-2} s^{-1}, \quad U_1 = 15 ms^{-1},$$
$$N_2 = 0.9 \times 10^{-2} s^{-1}, \quad U_2 = 25 ms^{-1},$$
$$N_3 = 2.0 \times 10^{-2} s^{-1}, \quad U_3 = 45 ms^{-1}.$$

For our model we need to construct these layers of buoyancy frequency out of layers of different density. Solving

$$\frac{\partial \rho}{\partial z} = -\frac{\rho}{g} N^2 \tag{4.23}$$

for ρ gives

$$\rho = e^{-N^2 z/g}. \tag{4.24}$$

Thus

$$\rho_i = e^{-N^2 z/g} \rho_{i-1}, \tag{4.25}$$

where the subscript i denotes the i^{th} layer. We can now build up the required N^2 profile. We use 10 layers of density to each layer of buoyancy frequency. The result is given in figure 4.4. It shows good agreement with figure 4.5. The steep drop over the mountain is well produced but, although the disturbance persists to higher levels the shape is not quite correct - the surface rises a little before it drops and this feature is not present in Klemp's result.

4.3.3 Variation of buoyancy frequancy

Figure 4.6: $d_i(x)$ for $m = 0.001m^{-1}$.

Figures 4.6 and 4.7 show $d_i(x)$ for two different values of m. The maximum amplitudes of the waves are greater in the case where m is smaller but this can be explained by the linear theory since the wave amplitudes are proportional to $\frac{F_0}{2(F_0-1)}$ which is larger if U_0 is. In order to investigate these differences further we plot the location of the maximum waves amplitues for both values of m, see figure 4.8. Again this is disappointing since there is little difference other than that which you would expect from a variation in wind speed.

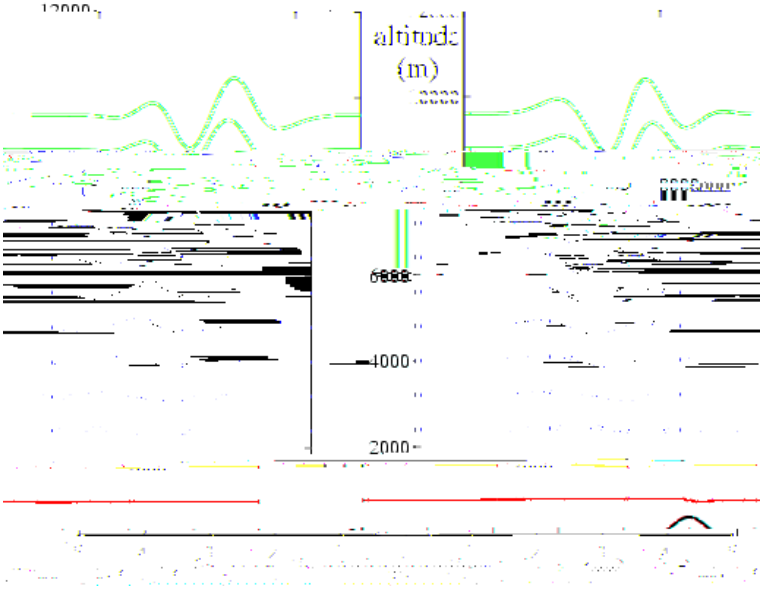

Figure 4.7: $d_i(x)$ for $m = 0.002m^{-1}$.

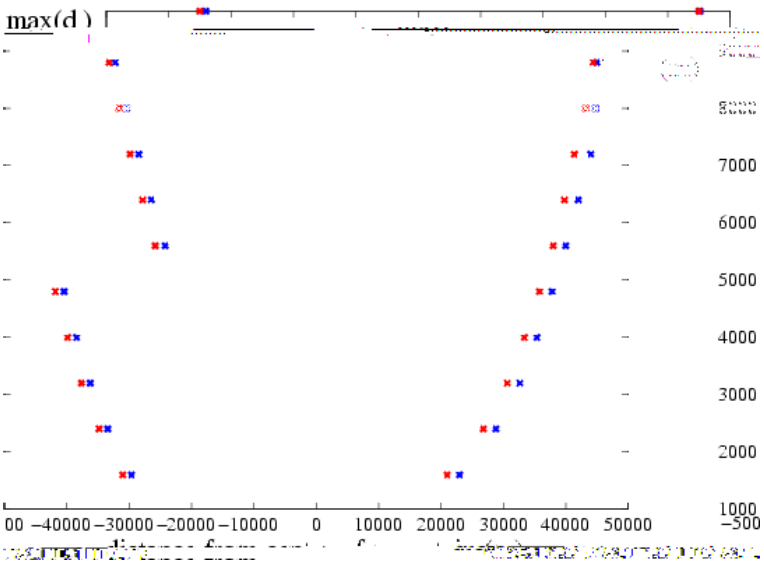

Figure 4.8: A comparison of the locations of the maximum wave amplitudes for $m = 0.001m^{-1}$ (blue) and $m = 0.002m^{-1}$ (red).

4.3.4 Vertical wind profile

In this section we investigate the effect of varying the initial wind speed with height as shown in figure 4.9.

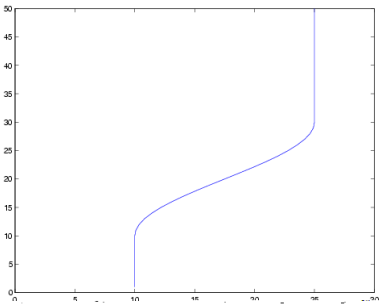

Figure 4.9: Initial vertical velocity profile, $U(z)$.

The results, shown in blue in figure 4.10, are not as expected. We were hoping to see some reflection at the layer where U is decreasing. The red curves show the result when the conditions are identical apart from the initial horizontal velocity which is a constant $10ms^{-1}$ for all z. There is some difference in the outputs above the critical layer, as is shown in figure 4.11, but it is believed that these differences are due purely to the different wind speed rather than to the fact that the waves have passed through a critical layer.

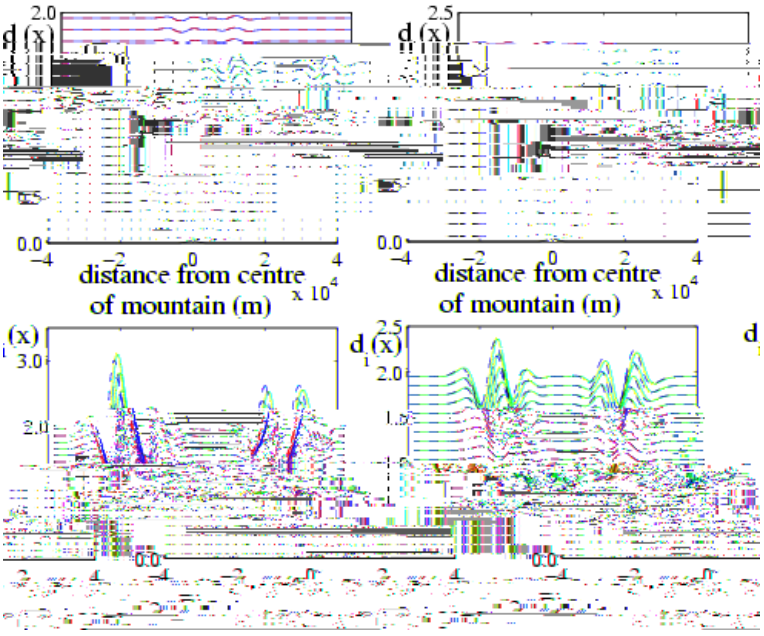

Figure 4.10: A comparison of $d_i(x)$ in the case where $U(z)$ is as given in figure 4.9 (blue), to the case where $U = 10ms^{-1}$ is constant with height (red).

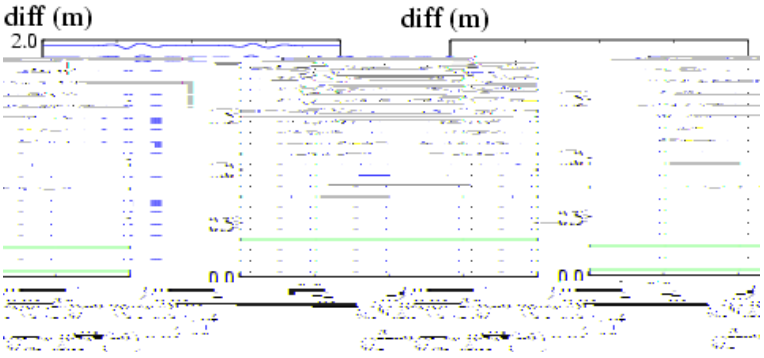

Figure 4.11: A plot of the difference between the two cases shown in figure 4.10, for the last two timeframes (before this there was little difference). As expected there is no difference below the critical layer but some difference above.

Chapter 5

Conclusions

This study has examined the importance of gravity waves in the atmosphere. The mechanism by which they are generated has been explained with particular emphasis on topographic forcing. The flow of a homogeneous layer over an isolated obstacle has been studied in detail and the numerical results agree well with those already established. The theory of stratified flow has been discussed and the numerical model extended to deal with multilayer, stratified flow. The results presented above have not been exactly as we envisaged and it is not clear that the multilayer system should exhibit the same characteristics as the continuously stratified flow it is attempting to represent.

5.1 Evaluation of the multilayer model

5.1.1 Resolution

The vertical resolution is of greater interest. In most cases the model has been run with all of the density layers having the same depth. The exception to this is the comparison with the Klemp and Lilly (1975) model where different layer depths were used in each of the levels of buoyancy frequency. Since this the case that produced the most encouraging results, it is likely that increasing the vertical resolution would have some positive effects. For example, Klemp and Lilly (1975) uses a vertical spacing based on the potential temperature. It may also be instructive to increase the resolution at critical layers. Perhaps the most obvious improvement would be to increase the depth of the first layer so that higher mountains could be modelled without losing resolution higher up in the atmosphere.

5.1.2 The sponge layer

The necessary presence of a sponge layer at the upper boundary greatly increases the run time of the program. However, some way of approximating the condition that waves radiate outwards must be implimented. Durran (1999) suggests another option which involves including a viscous term in the upper layers but this does not necessarily improve the situation since a wave absorbing layer must still be implemented.

5.1.3 The hydrostatic approximation

In the derivation of the equations of motion for a multilayer fluid we assumed the flow to be hydrostatic inorder to find an expression for the pressure within each layer. However, it is possible to represent nonhydrostatic flow using a multilayer model simply by retaining the vertical velocity variable w.

5.2 Further work

It is clear from the results presented in this study that more work is required before the multilayer model can be trusted to give reliable results. However, once the

model is workable, there are many other situations it can be applied to. These are outlined in the final sections below.

5.2.1 Layers with uniform density and vorticity

Following Baines (1995) we suggest that the layered model may better approximate a continuously stratified fluid if the velocity gradient, rather than the velocity, were uniform in each layer. Defining the mean velocity to be

$$U_i(z) = U(z_{(i-1)s}) + (z - z_{(i-1)s})\frac{dU_i}{dz}, \tag{5.1}$$

where z_{is} is the undisturbed height of the top of the i_{th} layer, we see that this new approximation would give a countinuous mean velocity profile. This is clearly a step closer to approximating a continuous velocity profile.

5.2.2 Rotational effects

Nappo (2002) makes the point that, since the hydrostatic approximation becomes more appropriate as the mountain width increases, there will come a point where the effects of the Earth's rotation will be felt. He calculates that a parcel travelling at $10ms^{-1}$iimakfects incr-akrange16hf 10ap597.97 Tf 40f 11.706 0 Td[(ms)]TJF1551

of the flow over a long ridge of constant cross section but even in this case it is evident that the ridge will end and the air will be able to flow around it. The characteristics of both two dimensional and fully three dimensional flow can be expected to be quite different from those of the simplified flow presented in this study.

Bibliography

J. R. Andrews, D. G.and Holton and C. B. Leovy. *Middle atmosphere dynamics*. Academic Press, 1987.

P. G. Baines. *Topographic Effects in Stratified Flows*. Cambridge Univ. Press, 1995.

G. A. Corby and C. E. Wallington. Airflow over mountains: the lee-wave amplitude. *Q. J. R. Meteorol. Soc.*, 82:266–274, 1956.

D. R. Durran. *Numerical methods for wave equations in geophysical fluid dynamics*. Springer-Verlag, 1999.

A. E. Gill. *Atmosphere-Ocean Dynamics*. Academic Press, 1982.

D. D. Houghton and A. Kasahara. Nonlinear shallow fluid flow over an isolated ridge. *Comm. Pure Appl. Math.*, 21:1–23, 1968.

J. B. Klemp and D. K. Lilly. The dynamics of wave induced downslope winds. *J.*

C. J. Nappo. *Atmospheric Gravity Waves*. Academic Press, 2002.

P. Queney. The problem of airflow over mountains: a summary of theoretical studies.